

## 1.4

### FIRST-PRINCIPLES MOLECULAR DYNAMICS

Roberto Car<sup>1</sup>, Filippo de Angelis<sup>2</sup>, Paolo Giannozzi<sup>3</sup>, and Nicola Marzari<sup>4</sup>

<sup>1</sup>*Department of Chemistry and Princeton Materials Institute, Princeton University, Princeton, NJ, USA*

<sup>2</sup>*Istituto CNR di Scienze e Tecnologie Molecolari ISTM, Dipartimento di Chimica, Università di Perugia, Via Elce di Sotto 8, I-06123, Perugia, Italy*

<sup>3</sup>*Scuola Normale Superiore and National Simulation Center, INFN-DEMOCRITOS, Pisa, Italy*

<sup>4</sup>*Department of Materials Science and Engineering, Massachusetts Institute of Technology, Cambridge, MA, USA*

*Ab initio* or first-principles methods have emerged in the last two decades as a powerful tool to probe the properties of matter at the microscopic scale. These approaches are used to derive macroscopic observables under the controlled condition of a “computational experiment,” and with a predictive power rooted in the quantum-mechanical description of interacting atoms and electrons. Density-functional theory (DFT) has become *de facto* the method of choice for most applications, due to its combination of reasonable scaling with system size and good accuracy in reproducing most ground state properties. Such an electronic-structure approach can then be combined with classical molecular dynamics to provide an accurate description of thermodynamic properties and phase stability, atomic dynamics, and chemical reactions, or as a tool to sample the features of a potential energy surface.

In a molecular-dynamics (MD) simulation the microscopic trajectory of each individual atom in the system is determined by integration of Newton’s equations of motion. In classical MD, the system is considered composed of massive, point-like nuclei, with forces acting between them derived from empirical effective potentials. *Ab initio* MD maintains the same assumption of treating atomic nuclei as classical particles; however, the forces acting on them are considered quantum mechanical in nature, and are derived from an electronic-structure calculation. The approximation of treating quantum-mechanically only the electronic subsystem is usually perfectly appropriate, due to the large difference in mass between electrons and nuclei. Nevertheless, nuclear quantum effects can be sometimes relevant, especially for light

elements such as hydrogen; classical or *ab initio path integral* approaches can then be applied, albeit at a higher computational cost. The use of Newton’s equations of motion for the nuclear evolution implies that vibrational degrees of freedom are not quantized, and will follow a Boltzmann statistics. This approximation becomes fully justified only for temperatures comparable with the highest vibrational level in the system considered.

In the following, we will describe the combined approach of Car and Parrinello to determine the simultaneous “on-the-fly” evolution of the (Newtonian) nuclear degrees of freedom and of the electronic wavefunctions, as implemented in a modern density-functional code [1] based on plane-waves basis sets, and with the electron–ion interactions described by ultrasoft pseudopotentials [2].

## 1. Total Energies and the Ultrasoft Pseudopotential Method

Within DFT, the ground-state energy of a system of  $N_v$  electrons, whose one-electron Kohn–Sham (KS) orbitals are  $\phi_i$ , is given by

$$E_{\text{tot}}[\{\phi_i\}, \{\mathbf{R}_I\}] = \sum_i \left\langle \phi_i \left| -\frac{\hbar^2}{2m} \nabla^2 + V_{\text{NL}} \right| \phi_i \right\rangle + E_{\text{H}}[n] + E_{\text{xc}}[n] + \int d\mathbf{r} V_{\text{loc}}^{\text{ion}}(\mathbf{r})n(\mathbf{r}) + U(\{\mathbf{R}_I\}), \quad (1)$$

where the  $i$  index runs over occupied KS orbitals ( $N_v/2$  for closed-shell systems) and  $n(\mathbf{r})$  is the electron density.  $E_{\text{H}}[n]$  is the Hartree energy defined as:

$$E_{\text{H}}[n] = \frac{e^2}{2} \iint d\mathbf{r} d\mathbf{r}' \frac{n(\mathbf{r})n(\mathbf{r}')}{|\mathbf{r} - \mathbf{r}'|}, \quad (2)$$

$E_{\text{xc}}[n]$  is the exchange and correlation energy,  $\mathbf{R}_I$  are the coordinates of the  $I$ th nucleus,  $\{\mathbf{R}_I\}$  is the set of all nuclear coordinates, and  $U(\{\mathbf{R}_I\})$  is the nuclear Coulomb interaction energy.

In typical first-principles MD implementations, pseudopotentials (PPs) are used to describe the interaction between the valence electrons and the ionic core, which includes the nucleus and the core electrons. The use of PPs allows to simplify the many-body electronic problem by avoiding an explicit description of the core electrons, which in turn results in a greatly reduced number of orbitals and allows the use of plane waves as a basis set. In the following, we will consider the general case of ultrasoft PPs [2], which includes as a special case norm-conserving PPs [3] in separable form. The PP is composed of a local part  $V_{\text{loc}}^{\text{ion}}$ , given by a sum of atom-centred radial potentials:

$$V_{\text{loc}}^{\text{ion}}(\mathbf{r}) = \sum_I V_{\text{loc}}^I(|\mathbf{r} - \mathbf{R}_I|) \quad (3)$$

and a nonlocal part  $V_{\text{NL}}$ :

$$V_{\text{NL}} = \sum_{nm,I} D_{nm}^{(0)} |\beta_n^I\rangle \langle \beta_m^I|, \quad (4)$$

where the functions  $\beta_n^I$  and the coefficients  $D_{nm}^{(0)}$  characterize the PP and are specific for each atomic species. For simplicity, we will consider only a single atomic species in the following. The  $\beta_n^I$  functions, centred at site  $\mathbf{R}_I$ , depend on the nuclear positions via

$$\beta_n^I(\mathbf{r}) = \beta_n(\mathbf{r} - \mathbf{R}_I). \quad (5)$$

$\beta_n$  here is a combination of an angular momentum eigenfunction in the angular variables times a radial function which vanishes outside the core region; the indices  $n$  and  $m$  in Eq. (4) run over the total number  $N_\beta$  of these functions.

The electron density entering Eq. (1) is given by

$$n(\mathbf{r}) = \sum_i \left[ |\phi_i(\mathbf{r})|^2 + \sum_{nm,I} Q_{nm}^I(\mathbf{r}) \langle \phi_i | \beta_n^I \rangle \langle \beta_m^I | \phi_i \rangle \right], \quad (6)$$

where the sum runs over occupied KS orbitals. The augmentation functions  $Q_{nm}^I(\mathbf{r}) = Q_{nm}(\mathbf{r} - \mathbf{R}_I)$  are localized in the core. The ultrasoft PP is fully determined by the quantities  $V_{\text{loc}}^I(r)$ ,  $D_{nm}^{(0)}$ ,  $Q_{nm}(\mathbf{r})$ , and  $\beta_n(\mathbf{r})$ . The functions  $Q_{nm}(\mathbf{r})$  are related to atomic orbitals via  $Q_{nm}(\mathbf{r}) = \psi_n^{ae*}(\mathbf{r}) \psi_m^{ae}(\mathbf{r}) - \psi_n^{ps*}(\mathbf{r}) \psi_m^{ps}(\mathbf{r})$ , where  $\psi^{ae}$  are the all-electron atomic orbitals (not necessarily bound), and  $\psi^{ps}$  are the corresponding pseudo-orbitals. The  $Q_{nm}(\mathbf{r})$  themselves can be smoothed for computational convenience, by taking a truncated multiple expansion [4]. For the case of norm-conserving PPs the  $Q_{nm}(\mathbf{r})$  are identically zero.

The KS orbitals obey generalized orthonormality conditions

$$\langle \phi_i | S(\{\mathbf{R}_I\}) | \phi_j \rangle = \delta_{ij}, \quad (7)$$

where  $S$  is a Hermitian overlap operator given by

$$S = 1 + \sum_{nm,I} q_{nm} |\beta_n^I\rangle \langle \beta_m^I|, \quad (8)$$

and

$$q_{nm} = \int d\mathbf{r} Q_{nm}(\mathbf{r}). \quad (9)$$

The orthonormality condition (7) is consistent with the conservation of the charge  $\int d\mathbf{r} n(\mathbf{r}) = N_v$ . Note that the overlap operator  $S$  depends on nuclear positions through the  $|\beta_n^I\rangle$ .

The ground-state orbitals  $\phi_i$  that minimize the total energy (1) subject to the constraints (7) are given by

$$\frac{\delta E_{\text{tot}}}{\delta \phi_i^*(\mathbf{r})} = \epsilon_i S \phi_i(\mathbf{r}), \quad (10)$$

where the  $\epsilon_i$  are Lagrange multipliers. Equation (10) yields the KS equations

$$H|\phi_i\rangle = \epsilon_i S|\phi_i\rangle, \quad (11)$$

where  $H$ , the KS Hamiltonian, is defined as

$$H = -\frac{\hbar^2}{2m}\nabla^2 + V_{\text{eff}} + \sum_{nm,I} D_{nm}^I |\beta_n^I\rangle \langle \beta_m^I|. \quad (12)$$

Here,  $V_{\text{eff}}$  is a screened effective local potential

$$V_{\text{eff}}(\mathbf{r}) = V_{\text{loc}}^{\text{ion}}(\mathbf{r}) + V_{\text{H}}(\mathbf{r}) + \mu_{\text{xc}}(\mathbf{r}), \quad (13)$$

$\mu_{\text{xc}}(\mathbf{r})$  is the exchange-correlation potential

$$\mu_{\text{xc}}(\mathbf{r}) = \frac{\delta E_{\text{xc}}[n]}{\delta n(\mathbf{r})}, \quad (14)$$

and  $V_{\text{H}}(\mathbf{r})$  is the Hartree potential

$$V_{\text{H}}(\mathbf{r}) = e^2 \int d\mathbf{r}' \frac{n(\mathbf{r}')}{|\mathbf{r} - \mathbf{r}'|}. \quad (15)$$

The ‘‘screened’’ coefficients  $D_{nm}^I$  appearing in Eq. (12) are defined as

$$D_{nm}^I = D_{nm}^{(0)} + \int d\mathbf{r} V_{\text{eff}}(\mathbf{r}) Q_{nm}^I(\mathbf{r}). \quad (16)$$

The  $D_{nm}^I$  depend on the KS orbitals through  $V_{\text{eff}}$  (Eq. (13)) and the charge density  $n(\mathbf{r})$  (Eq. (6)). Since the KS Hamiltonian in Eq. (11) depends on the KS orbitals  $\phi_i$  via the charge density, the solution of Eq. (11) is achieved by an iterative self-consistent field procedure.

## 2. First-Principles Molecular Dynamics: Born–Oppenheimer and Car–Parrinello

We will assume here that all nuclei (together with their core electrons) can be treated as classical particles; furthermore, we consider only systems for which a separation between the classical motion of the atoms and the quantum motion of the electrons can be achieved, i.e., systems satisfying the

Born–Oppenheimer adiabatic approximation. For any given ionic configurations, it is possible to calculate the self-consistent electronic ground state, and consequently the forces acting on the ions by virtue of the Hellmann–Feynman theorem. The knowledge of the ionic forces allows then to evolve the nuclear trajectories in time, using any of the algorithms developed in classical mechanics for finite-differences solution of Newton’s equations of motion (two of the most popular choices are Verlet algorithms and Gear predictor–corrector approaches). Born–Oppenheimer MD strives for an accurate evolution of the ions by alternatively converging the electronic wavefunctions to full selfconsistency, for a given set of nuclear coordinates, and then evolving by a finite time step the ions according to the quantum mechanical forces acting on them. A practical algorithms could be summarized as such:

- self-consistent solution of the KS equations for a given ionic configuration  $\{\mathbf{R}_I\}$ ;
- calculation of the forces acting on the nuclei via the Hellmann–Feynman theorem;
- integration of the Newton’s equations of motion for the nuclei;
- update of the ionic configuration.

This way, the nuclei move on the Born–Oppenheimer surface, i.e., with the electrons in their ground state for any instantaneous configuration of the  $\{\mathbf{R}_I\}$ . An efficient implementation of this class of algorithms relies on efficient self-consistent minimization schemes for the electronic wavefunctions, and on accurate extrapolations of the electronic ground-state from one step to the other. The time step itself will only be limited by the need to integrate accurately the highest ionic frequencies. In addition, due to the impossibility of reaching perfect electronic selfconsistency, a drift of the constant of motion is unavoidable, and long simulations require the use of a thermostat to compensate.

On the other hand, the Car–Parrinello approach [5] combines “on-the-fly” the simultaneous classical MD evolution of the atomic nuclei with the determination of the ground-state wavefunction for the electrons. A (fictitious) dynamics for the electronic degrees of freedom is introduced, defining a classical Lagrangian for the combined electronic and ionic degrees of freedom

$$\mathcal{L} = \mu \sum_i \int d\mathbf{r} |\dot{\phi}_i(\mathbf{r})|^2 + \frac{1}{2} \sum_I M_I \dot{\mathbf{R}}_I^2 - E_{\text{tot}}(\{\phi_i\}, \{\mathbf{R}_I\}); \quad (17)$$

the wavefunctions above are subject to the set of orthonormality constraints

$$\mathcal{N}_{ij}(\{\phi_i\}, \{\mathbf{R}_I\}) = \langle \phi_i | S(\{\mathbf{R}_I\}) | \phi_j \rangle - \delta_{ij} = 0. \quad (18)$$

Here,  $\mu$  is a mass parameter coupled to the electronic degrees of freedom,  $M_I$  are the masses of the atoms, and  $E_{\text{tot}}$  and  $S$  were given in Eqs. (1) and (8),

respectively. The first term in Eq. (17) plays the role of a kinetic energy associated to the electronic degrees of freedom. The orthonormality constraints (18) are holonomic and do not lead to energy dissipation in a MD run.

The Euler equations of motion generated by the Lagrangian of Eq. (17) under the constraints (18) are:

$$\mu\ddot{\phi}_i = -\frac{\delta E_{\text{tot}}}{\delta \phi_i^*} + \sum_j \Lambda_{ij} S\phi_j, \quad (19)$$

$$\mathbf{F}_I = M_I \ddot{\mathbf{R}}_I = -\frac{\partial E_{\text{tot}}}{\partial \mathbf{R}_I} + \sum_{ij} \Lambda_{ij} \left\langle \phi_i \left| \frac{\partial S}{\partial \mathbf{R}_I} \right| \phi_j \right\rangle. \quad (20)$$

where  $\Lambda_{ij}$  are Lagrange multipliers enforcing orthogonality. If the system is in the electronic ground state corresponding to the nuclear configuration at that time step, the forces acting on the electronic degrees of freedom  $\mu\dot{\phi}_i=0$  vanish and Eq. (19) reduces to the KS equations (10) or (11). A unitary rotation brings the  $\Lambda$  matrix into diagonal form:  $\Lambda_{ij} = \epsilon_i \delta_{ij}$ .

Similarly, the equilibrium nuclear configuration is achieved when the atomic forces  $\mathbf{F}_I$  in Eq. (20) vanish. In deriving explicit expressions for the forces, Eq. (20), one should keep in mind that the electron density also depends on  $\mathbf{R}_I$  through  $Q_{nm}^I$  and  $\beta_n^I$ . Introducing the quantities

$$\rho_{nm}^I = \sum_i \langle \phi_i | \beta_n^I \rangle \langle \beta_m^I | \phi_i \rangle, \quad (21)$$

and

$$\omega_{nm}^I = \sum_{ij} \Lambda_{ij} \langle \phi_j | \beta_n^I \rangle \langle \beta_m^I | \phi_i \rangle, \quad (22)$$

we arrive at the expression

$$\begin{aligned} \mathbf{F}_I = & -\frac{\partial U}{\partial \mathbf{R}_I} - \int d\mathbf{r} \frac{\partial V_{\text{loc}}^{\text{ion}}}{\partial \mathbf{R}_I} n(\mathbf{r}) - \int d\mathbf{r} V_{\text{eff}}(\mathbf{r}) \sum_{nm} \frac{\partial Q_{nm}^I(\mathbf{r})}{\partial \mathbf{R}_I} \rho_{nm}^I \\ & - \sum_{nm} D_{nm}^I \frac{\partial \rho_{nm}^I}{\partial \mathbf{R}_I} + \sum_{nm} q_{nm} \frac{\partial \omega_{nm}^I}{\partial \mathbf{R}_I}, \end{aligned} \quad (23)$$

where  $D_{nm}^I$  and  $V_{\text{eff}}$  have been defined in Eqs. (16) and (13), respectively. The last term of Eq. (23) gives the constraint contribution to the forces.

We underline that the dynamical evolution for the electronic degrees of freedom should not be construed as representing the true electron dynamics; rather it represent a dynamical system of fictitious degree of freedom adiabatically decoupled from the moving ions, but driven to follow closely the ionic dynamics, with small and oscillatory departures from what would be the exact Born–Oppenheimer ground-state energy. As a consequence, even

the Car–Parrinello dynamics for the nuclei becomes in principle inequivalent to the Born–Oppenheimer dynamics. However, suitable choices for the computational parameters used in the simulation exist, and are such that the two dynamics give the same macroscopic observables. The full self-consistency cycle of the Born–Oppenheimer dynamics can be dispensed for, at a great computational advantage only marginally offset by the need to use shorter timesteps to integrate the fast electronic degrees of freedom.

The adiabatic separation can be understood on the basis of the following argument [6, 7]. The fictitious electronic dynamics, once close to the ground state, can be described as a superposition of harmonic oscillators whose frequencies are given by:

$$\omega_{ij} = \left[ \frac{2(\epsilon_j - \epsilon_i)}{\mu} \right]^{1/2}, \quad (24)$$

where  $\epsilon_i$  is the KS eigenvalue of the  $i$ th occupied orbital and  $\epsilon_j$  is the KS eigenvalue of the  $j$ th unoccupied orbital. For a system with an energy gap  $E_g$ , the lowest frequency can be estimated to be  $\omega_{\min} = (2E_g/\mu)^{1/2}$ . If  $\omega_{\min}$  is much larger than the highest frequency appearing in the nuclear motion, there is a large separation between electronic and nuclear frequencies. Under such conditions, the electronic motion is adiabatically decoupled from the nuclear motion and there is negligible energy transfer from nuclear to electronic degrees of freedom. This is a nonobvious result, since both dynamics are classical and subject to the equipartition of energy, and it is the key to understand when and why the Car–Parrinello dynamics works.

For typical  $E_g$  values, in the order of a few electronvolts, the electronic mass parameter  $\mu$  can be chosen relatively large, in the order of 300–500 amu or even more, without any loss of adiabaticity. The time step of the simulation can be chosen as the largest compatible with the resulting electronic dynamics. Larger values of  $\mu$  allow the use of larger time steps, but the requirement of adiabaticity sets an upper limit to  $\mu$ . Time steps of a fraction of a femtosecond are typically accessible. The electronic dynamics is faster than the nuclear dynamics and averages out the error on forces that is present because the system is never at the instantaneous electronic ground state, but only close to it (the system has to be brought close to the electronic ground state at the beginning of the dynamics). In such conditions, the resulting nuclear dynamics is very close to the true Born–Oppenheimer dynamics, and the electronic dynamics is stable (with negligible energy transfer from the nuclei) even for long simulation times. Moreover, the Car–Parrinello dynamics is computationally more convenient than the Born–Oppenheimer dynamics, because the latter requires a high accuracy in self-consistency in order to provide the needed accuracy on the forces. The Car–Parrinello dynamics does not provide accurate instantaneous forces, but it provides accurate average nuclear trajectories.

## 2.1. Equations of Motion and Orthonormality Constraints

In Car–Parrinello implementations equations of motion (19) and (20) are discretized using the standard-Verlet or the velocity-Verlet algorithm. The following discussion, including the treatment of the  $\mathbf{R}_I$ -dependence of the orthonormality constraints, applies to the standard Verlet algorithm, and using the Fourier acceleration scheme of Tassone *et al.* [8]. (In this approach the fictitious electronic mass is generally represented by an operator  $\Theta$ , chosen in such a way to reduce the highest electronic frequencies. \*)

From the knowledge of the electronic orbitals at time  $t$  and  $t - \Delta t$ , the orbitals at  $t + \Delta t$  are given, in the standard Verlet, by

$$\begin{aligned} \phi_i(t + \Delta t) = & 2\phi_i(t) - \phi_i(t - \Delta t) \\ & - (\Delta t)^2 \Theta^{-1} \left[ \frac{\delta E_{\text{tot}}}{\delta \phi_i^*} - \sum_j \Lambda_{ij}(t + \Delta t) S(t) \phi_j(t) \right]; \end{aligned} \quad (25)$$

where  $\Delta t$  is the time step, and  $S(t)$  indicates the operator  $S$  evaluated for nuclear positions  $\mathbf{R}_I(t)$ . Similarly the nuclear coordinates at time  $t + \Delta t$  are given by:

$$\begin{aligned} \mathbf{R}_I(t + \Delta t) = & 2\mathbf{R}_I(t) - \mathbf{R}_I(t - \Delta t) - \frac{(\Delta t)^2}{M_I} \\ & \times \left[ \frac{\partial E_{\text{tot}}}{\partial \mathbf{R}_I} - \sum_{ij} \Lambda_{ij}(t + \Delta t) \left\langle \phi_i(t) \left| \frac{\partial S(t)}{\partial \mathbf{R}_I} \right| \phi_j(t) \right\rangle \right]. \end{aligned} \quad (26)$$

The orthonormality conditions must be imposed at each time-step:

$$\langle \phi_i(t + \Delta t) | S(t + \Delta t) | \phi_j(t + \Delta t) \rangle = \delta_{ij}, \quad (27)$$

leading to the following matrix equation:

$$A + \lambda B + B^\dagger \lambda^\dagger + \lambda C \lambda^\dagger = 1 \quad (28)$$

where the unknown matrix  $\lambda$  is related to the matrix of Lagrange multipliers  $\Lambda$  at time  $t + \Delta t$  via  $\lambda = (\Delta t)^2 \Lambda^*(t + \Delta t)$ . In Eq. (28), the dagger indicates

\*When using plane waves, a convenient choice for the matrix elements of such operator is  $\Theta_{\mathbf{G}, \mathbf{G}'} = \max(\mu, \mu((\hbar^2 G^2)/(2mE_c))) \delta_{\mathbf{G}, \mathbf{G}'}$ , where  $\mathbf{G}, \mathbf{G}'$  are the wave vector of PWs,  $E_c$  is a cutoff (typically a few Ry) which defines the threshold for Fourier acceleration. The fictitious electron mass depends on  $G$  as the kinetic energy for large  $G$ , it is constant for small  $G$ . This scheme allows us to use larger steps with negligible computational overhead.

Hermitian conjugate ( $\lambda = \lambda^\dagger$ ). The matrices  $A$ ,  $B$ , and  $C$  are given by:

$$\begin{aligned} A_{ij} &= \langle \bar{\phi}_i | S(t + \Delta t) | \bar{\phi}_j \rangle, \\ B_{ij} &= \langle \Theta^{-1} S(t) \phi_i(t) | S(t + \Delta t) | \bar{\phi}_j \rangle, \\ C_{ij} &= \langle \Theta^{-1} S(t) \phi_i(t) | S(t + \Delta t) | \Theta^{-1} S(t) \phi_j(t) \rangle, \end{aligned} \quad (29)$$

with

$$\bar{\phi}_i = 2\phi_i(t) - \phi_i(t - \Delta t) - (\Delta t)^2 \Theta^{-1} \frac{\delta E_{\text{tot}}(t)}{\delta \phi_i^*}. \quad (30)$$

The solution of Eq. (28) in the ultrasoft PP case is not obvious, because Eq. (26) is not a closed expression for  $\mathbf{R}_I(t + \Delta t)$ . The problem is that  $\Lambda(t + \Delta t)$  appearing in Eq. (26) depends implicitly on  $\mathbf{R}_I(t + \Delta t)$  through  $S(t + \Delta t)$ . Consequently, it is in principle necessary to solve iteratively for  $\mathbf{R}_I(t + \Delta t)$  in Eq. (26).

A simple solution to this problem was provided in Laasonen *et al.* [4].  $\Lambda(t + \Delta t)$  is extrapolated using two previous values:

$$\Lambda_{ij}^{(0)}(t + \Delta t) = 2\Lambda_{ij}(t) - \Lambda_{ij}(t - \Delta t). \quad (31)$$

Equation (26) is used to find  $\mathbf{R}_I^{(0)}(t + \Delta t)$ , which is correct to  $O(\Delta t^4)$ . From  $\mathbf{R}_I^{(0)}(t + \Delta t)$  we can obtain a new set  $\Lambda_{ij}^{(1)}(t + \Delta t)$  and repeat the procedure until convergence is achieved. It turns out that in most practical applications the procedure converges at the very first iteration. Thus, the operations described above are generally executed only once per time step.

The solution of Eq. (28) is found using a modified version [4, 9] of the iterative procedure of Car and Parrinello [10]. The matrix  $B$  is decomposed into hermitian ( $B_h$ ) and antihermitian ( $B_a$ ) parts,

$$B = B_h + B_a, \quad (32)$$

and the solution is obtained by iteration:

$$\lambda^{(n+1)} B_h + B_h \lambda^{(n+1)} = 1 - A - \lambda^{(n)} B_a - B_a^\dagger \lambda^{(n)} - \lambda^{(n)} C \lambda^{(n)}. \quad (33)$$

The initial guess  $\lambda^{(0)}$  can be obtained from

$$\lambda^{(0)} B_h + B_h \lambda^{(0)} = 1 - A. \quad (34)$$

Here, the  $B_a$ - and  $C$ -dependent terms are neglected because they are of higher order in  $\Delta t$  ( $B_a$  vanishes for vanishing  $\Delta t$ ). Equations (34) and (33) have the same structure:

$$\lambda B_h + B_h \lambda = X \quad (35)$$

where  $X$  a Hermitian matrix. Equation (35) can be solved exactly by finding the unitary matrix  $U$  that diagonalizes  $B_h$ :  $U^\dagger B_h U = D$ , where  $D_{ij} = d_i \delta_{ij}$ . The solution is obtained from

$$(U^\dagger \lambda U)_{ij} = (U^\dagger X U)_{ij} / (d_i + d_j). \quad (36)$$

When  $X = 1 - A$ , Eq. (36) yields the starting  $\lambda^{(0)}$ , while  $\lambda^{(n+1)}$  is obtained from  $\lambda^{(n)}$  by solving Eq. (36) with  $X$  given by Eq. (33). This iterative procedure usually converges in very few steps (ten or less).

### 3. Plane-Wave Implementation

In most standard implementations, first-principles MD schemes employ a plane-wave (PW) basis set. An advantage of PWs is that they do not depend on atomic positions and are free of basis-set superposition errors. Total energies and forces on the atoms can be calculated using computationally efficient Fast Fourier transform (FFT) techniques and Pulay forces [11] vanish because PWs do not depend on atomic positions. Finally, the convergence of a calculation can be controlled in a simple way, since it depends only upon the number of PWs included in the expansion of the electron density. The dimension of a PW basis set is controlled by a cutoff in the kinetic energy of the PWs. A disadvantage of PWs is their extremely slow convergence in describing core states, which can however be circumvented by the use of PPs. Ultrasoft PPs allow to efficiently deal with this difficulty also in systems containing transition metals or first-row elements O, N, F whose 3d and 2p orbitals, respectively, are very contracted. The use of a PW basis set implies that periodic boundary conditions are imposed. Systems not having translational symmetry in one or more directions, have to be placed into a suitable periodically repeated box (a ‘‘supercell’’). Let  $\{\mathbf{R}\}$  be the translation vectors of the periodically repeated supercell. The corresponding reciprocal lattice vectors  $\{\mathbf{G}\}$  obey the conditions  $\mathbf{R}_i \cdot \mathbf{G}_j = 2\pi n$ , with  $n$  an integer number. The KS orbitals can be expanded in a plane-wave basis up to a kinetic energy cutoff  $E_c^{\text{wf}}$ :

$$\phi_{j,\mathbf{k}}(\mathbf{r}) = \frac{1}{\sqrt{\Omega}} \sum_{\mathbf{G} \in \{\mathbf{G}_c^{\text{wf}}\}} \phi_{j,\mathbf{k}}(\mathbf{G}) e^{-i(\mathbf{k}+\mathbf{G})\cdot\mathbf{r}}, \quad (37)$$

where  $\Omega$  is the volume of the cell,  $\{\mathbf{G}_c^{\text{wf}}\}$  is the set of  $\mathbf{G}$  vectors satisfying the condition

$$\frac{\hbar^2}{2m} |\mathbf{k} + \mathbf{G}|^2 < E_c^{\text{wf}}, \quad (38)$$

and  $\mathbf{k}$  is the Bloch vector of the electronic states. In crystals, one must use a grid of  $\mathbf{k}$ -points dense enough to sample the Brillouin zone (the unit cell of the

reciprocal lattice). In molecules, liquids and in general if the simulation cell is large enough, the Brillouin zone can be sampled using only the  $\mathbf{k} = 0$  ( $\Gamma$ ) point. An advantage of this choice is that the orbitals can be taken to be real in  $\mathbf{r}$ -space. In the following we will drop the  $\mathbf{k}$  vector index. Functions in real space and their Fourier transforms will be denoted by the symbols, if this does not originate ambiguity.

The  $\phi_j(\mathbf{G})$ s are the actual electronic variables in the fictitious dynamics. The calculation of  $H\phi_j$  and of the forces acting on the ions are the basic ingredients of the computation. Scalar products  $\langle \phi_j | \beta_n^I \rangle$  and their spatial derivatives are typically evaluated in  $\mathbf{G}$ -space. An important advantage of working in  $\mathbf{G}$ -space is that atom-centred functions like  $\beta_n^I$  and  $Q_{nm}^I$  are easily evaluated at any atomic position:

$$\beta_n^I(\mathbf{G}) = \beta_n(\mathbf{G})e^{-i\mathbf{G}\cdot\mathbf{R}_I}. \quad (39)$$

Thus,

$$\langle \phi_j | \beta_n^I \rangle = \sum_{\mathbf{G} \in \{\mathbf{G}_c^{\text{wf}}\}} \phi_j^*(\mathbf{G})\beta_n(\mathbf{G})e^{-i\mathbf{G}\cdot\mathbf{R}_I} \quad (40)$$

and

$$\left\langle \phi_j \left| \frac{\partial \beta_n^I}{\partial \mathbf{R}_I} \right. \right\rangle = -i \sum_{\mathbf{G} \in \{\mathbf{G}_c^{\text{wf}}\}} \mathbf{G} \phi_j^*(\mathbf{G})\beta_n(\mathbf{G})e^{-i\mathbf{G}\cdot\mathbf{R}_I}. \quad (41)$$

The kinetic energy term is diagonal in  $\mathbf{G}$ -space and is easily calculated:

$$-\left(\nabla^2 \phi_j\right)(\mathbf{G}) = G^2 \phi_j(\mathbf{G}). \quad (42)$$

In summary, the kinetic and nonlocal PP terms in  $H\phi_j$  are calculated in  $\mathbf{G}$ -space, while the local potential term  $V_{\text{eff}}\phi_j$ , that could be calculated in  $\mathbf{G}$ -space, is more conveniently determined using a ‘dual space’ technique, switching from  $\mathbf{G}$ - to  $\mathbf{r}$ -space with FFTs, and performing the calculation in the space where it is least expensive. In practice, the KS orbitals are first Fourier-transformed to  $\mathbf{r}$ -space; then,  $(V_{\text{eff}}\phi_j)(\mathbf{r}) = V_{\text{eff}}(\mathbf{r})\phi_j(\mathbf{r})$  is calculated in  $\mathbf{r}$ -space, where  $V_{\text{eff}}$  is diagonal; finally  $(V_{\text{eff}}\phi_j)(\mathbf{r})$  is Fourier-transformed back to  $(V_{\text{eff}}\phi_j)(\mathbf{G})$ . In order to use FFT, the  $\mathbf{r}$ -space is discretized by a uniform grid spanning the unit cell:

$$f(m_1, m_2, m_3) \equiv f(\mathbf{r}_{m_1, m_2, m_3}), \quad \mathbf{r}_{m_1, m_2, m_3} = m_1 \frac{\mathbf{a}_1}{N_1} + m_2 \frac{\mathbf{a}_2}{N_2} + m_3 \frac{\mathbf{a}_3}{N_3}, \quad (43)$$

where  $\mathbf{a}_1, \mathbf{a}_2, \mathbf{a}_3$  are lattice basis vectors, the integer index  $m_1$  runs from 0 to  $N_1 - 1$ , and similarly for  $m_2$  and  $m_3$ . In the following we will assume

for simplicity that  $N_1, N_2, N_3$  are even numbers. The FFT maps a discrete periodic function in real space  $f(m_1, m_2, m_3)$  into a discrete periodic function in reciprocal space  $\tilde{f}(n_1, n_2, n_3)$  (where  $n_1$  runs from 0 to  $N_1 - 1$ , and similarly for  $n_2$  and  $n_3$ ), and vice versa.

The link between  $\mathbf{G}$ -space components and FFT indices is:

$$\tilde{f}(n_1, n_2, n_3) \equiv f(\mathbf{G}_{n'_1, n'_2, n'_3}), \quad \mathbf{G}_{n'_1, n'_2, n'_3} = n'_1 \mathbf{b}_1 + n'_2 \mathbf{b}_2 + n'_3 \mathbf{b}_3 \quad (44)$$

where  $n_1 = n'_1$  if  $n'_1 \geq 0$ ,  $n_1 = n'_1 + N_1$  if  $n'_1 < 0$ , and similarly for  $n_2$  and  $n_3$ . The FFT dimensions  $N_1, N_2, N_3$  must be big enough to include all non negligible Fourier components of the function to be transformed: ideally the Fourier component corresponding to  $n'_1 = N_1/2$ , and similar for  $n'_2$  and  $n'_3$ , should vanish. In the following, we will refer to the set of indices  $n_1, n_2, n_3$  and to the corresponding Fourier components as the ‘‘FFT grid’’.

The soft part of the charge density  $n_{\text{soft}}(\mathbf{r}) = \sum_j |\phi_j(\mathbf{r})|^2$  contains Fourier components up to a kinetic energy cutoff  $E_c^{\text{soft}} = 4E_c^{\text{wf}}$ . This is evident from the formula:

$$n_{\text{soft}}(\mathbf{G}) = \sum_{\mathbf{G}' \in \{\mathbf{G}_c^{\text{wf}}\}} \sum_j \phi_j^*(\mathbf{G} - \mathbf{G}') \phi_j(\mathbf{G}'). \quad (45)$$

In the case of norm-conserving PPs, the entire charge density is given by  $n_{\text{soft}}(\mathbf{r})$ .

$V_{\text{eff}}$  should be expanded up to the same  $E_c^{\text{soft}}$  cutoff since all the Fourier components of  $V_{\text{eff}} \phi_j$  up to  $E_c^{\text{wf}}$  are required. Let us call  $\{\mathbf{G}_c^{\text{soft}}\}$  the set of  $\mathbf{G}$ -vectors such that

$$\frac{\hbar}{2m} G^2 < E_c^{\text{soft}}. \quad (46)$$

The soft part of the charge density is calculated in  $\mathbf{r}$ -space, by Fourier-transforming  $\phi_j(\mathbf{G})$  into  $\phi_j(\mathbf{r})$  and summing over the occupied states.

The exchange-correlation potential  $\mu_{\text{xc}}(\mathbf{r})$ , Eq. (14), is a function of the local charge density and – for gradient-corrected functionals – of its gradient at point  $\mathbf{r}$ :

$$\mu_{\text{xc}}(\mathbf{r}) = V_{\text{xc}}(n(\mathbf{r}), |\nabla n(\mathbf{r})|). \quad (47)$$

The gradient  $\nabla n(\mathbf{r})$  is conveniently calculated from the charge density in  $\mathbf{G}$ -space, using  $(\nabla n)(\mathbf{G}) = -i \mathbf{G} n(\mathbf{G})$ . The Hartree potential  $V_{\text{H}}(\mathbf{r})$ , Eq. (15), is also conveniently calculated in  $\mathbf{G}$ -space:

$$V_{\text{H}}(\mathbf{G}) = \frac{4\pi}{\Omega} \frac{n(\mathbf{G})^*}{G^2}. \quad (48)$$

Thus, in the case of norm-conserving PPs, a single FFT grid, large enough to accommodate the  $\{\mathbf{G}_c^{\text{soft}}\}$  set, can be used for orbitals, charge density, and potential.

The use of FFT is mathematically equivalent to a pure  $\mathbf{G}$ -space description (we neglect here a small inconsistency in exchange-correlation potential and energy density, due to the presence of a small amount of components beyond the  $\{\mathbf{G}_c^{\text{soft}}\}$  set). This has important consequences: working in  $\mathbf{G}$ -space means that translational invariance is exactly conserved and that forces are analytical derivatives of the energy (apart from the effect of the small inconsistency mentioned above). Forces that are analytical derivatives of the energy ensure that the constant of motion (i.e., the sum of kinetic and potential energy of the ions in Newtonian dynamics) is conserved during the evolution.

### 3.1. Double-Grid Technique

Let us focus on ultrasoft PPs. In  $\mathbf{G}$ -space the charge density is:

$$n(\mathbf{G}) = n_{\text{soft}}(\mathbf{G}) + \sum_{i,nm,l} Q_{mn}^l(\mathbf{G}) \langle \phi_i | \beta_n^l \rangle \langle \beta_m^l | \phi_i \rangle. \quad (49)$$

The augmentation term often requires a cutoff higher than  $E_c^{\text{soft}}$ , and as a consequence a larger set of  $\mathbf{G}$ -vectors. Let us call  $\{\mathbf{G}_c^{\text{dens}}\}$  the set of  $\mathbf{G}$ -vectors that are needed for the augmented part:

$$\frac{\hbar^2}{2m} G^2 < E_c^{\text{dens}}. \quad (50)$$

In typical situations, using pseudized augmented charges,  $E_c^{\text{dens}}$  ranges from  $E_c^{\text{soft}}$  to  $\sim 2 - 3 E_c^{\text{soft}}$ .

The same FFT grid could be used both for the augmented charge density and for KS orbitals. This however would imply using an oversized FFT grid in the most expensive part of the calculation, dramatically increasing computer time. A better solution is to introduce two FFT grids:

- a coarser grid (in  $\mathbf{r}$ -space) for the KS orbitals and the soft part of the charge density. The FFT dimensions  $N_1, N_2, N_3$  of this grid are big enough to accommodate all  $\mathbf{G}$ -vectors in  $\{\mathbf{G}_c^{\text{soft}}\}$ ;
- a denser grid (in  $\mathbf{r}$ -space) for the total charge density and the exchange-correlation and Hartree potentials. The FFT dimensions  $M_1 \geq N_1, M_2 \geq N_2, M_3 \geq N_3$  of this grid are big enough to accommodate all  $\mathbf{G}$ -vectors in  $\{\mathbf{G}_c^{\text{dens}}\}$ .

In this framework, the soft part of the electron density  $n_{\text{soft}}$ , is calculated in  $\mathbf{r}$ -space using FFTs on the coarse grid and transformed in  $\mathbf{G}$ -space using a coarse-grid FFT on the  $\{\mathbf{G}_c^{\text{soft}}\}$  grid. The augmented charge density is calculated in  $\mathbf{G}$ -space on the  $\{\mathbf{G}_c^{\text{dens}}\}$  grid, using Eq. (49) as described in the next section.  $n(\mathbf{G})$  is used to evaluate the Hartree potential, Eq. (48). Then

$n(\mathbf{G})$  is Fourier-transformed in  $\mathbf{r}$ -space on the dense grid, where the exchange-correlation potential, Eq. (47), is evaluated.

In real space, the two grids are not necessarily commensurate. Whenever the need arises to go from the coarse to the dense grid, or vice versa, this is done in  $\mathbf{G}$ -space. For instance, the potential  $V_{\text{eff}}$ , Eq. (13), is needed both on the dense grid to calculate quantities such as the  $D_{nm}^I$ , Eq. (16), and on the coarse grid to calculate  $V_{\text{eff}}\phi_j$ , Eq. (11). The connection between the two grids occurs in  $\mathbf{G}$ -space, where Fourier filtering is performed:  $V_{\text{eff}}$  is first transformed in  $\mathbf{G}$ -space on the dense grid, then transferred to the coarse  $\mathbf{G}$ -space grid by eliminating components incompatible with  $E_c^{\text{soft}}$ , and then back-transformed in  $\mathbf{r}$ -space using a coarse-grid FFT.

We remark that for each time step only a few dense-grid FFT are performed, while the number of necessary coarse-grid FFTs is much larger, proportional to the number of KS states  $N_{\text{ks}}$ .

### 3.2. Augmentation Boxes

Let us consider the augmentation functions  $Q_{nm}$ , which appear in the calculation of the electron density, Eq. (49), in the calculation of  $D_{nm}^I$ , Eq. (16), and in the integrals involving  $\partial Q_{nm}^I / \partial \mathbf{R}_I$  needed to compute the forces acting on the nuclei, Eq. (23). The calculation of the  $Q_{nm}$  in  $\mathbf{G}$ -space has a large computational cost because the cutoff for the  $Q_{nm}$  is the large cutoff  $E_c^{\text{dens}}$ . The computational cost can be significantly reduced if we take advantage of the localization of the  $Q_{nm}$  in the core region.

We call ‘‘augmentation box’’ a fraction of the supercell, containing a small portion of the dense grid in real space. An augmentation box is defined only for atoms described by ultrasoft PPs. The augmentation box for atom  $I$  is centred at the point of the dense grid that is closer to the position  $\mathbf{R}_I$ . During a MD run, the centre of the  $I$ th augmentation box makes discontinuous jumps to one of the neighbouring grid points whenever the position vector  $\mathbf{R}_I$  gets closer to such grid point. In a MD run, the augmentation box must always contain completely the augmented charge belonging to the  $I$ th atom; otherwise, the augmentation box must be as small as possible.

The volume of the augmentation box is much smaller than the volume of the supercell. The number of  $\mathbf{G}$ -vectors in the reciprocal space of the augmentation box is smaller than the number of  $\mathbf{G}$ -vectors in the dense grid by the ratio of the volumes of the augmentation box and of the supercell. As a consequence, the cost of calculations on the augmentation boxes increases linearly with the number of atoms described by ultrasoft PPs.

Augmentation boxes are used (i) to construct the augmented charge density, Eq. (6), and (ii) to calculate the self-consistent contribution to the

coefficients of the nonlocal PP, Eq. (16). In case (i), the augmented charge is conveniently calculated in  $\mathbf{G}$ -space, following [4], and Fourier-transformed in  $\mathbf{r}$ -space. All these calculations are done on the augmentation box grid. Then the calculated contribution at each  $\mathbf{r}$ -point of the augmentation box grid is added to the charge density at the same point in the dense grid. In case (ii), it is convenient to calculate  $D_{nm}^I$  as follows: for every atom described by a ultrasoft PP, take the Fourier transform of  $V_{\text{eff}}(\mathbf{r})$  on the corresponding augmentation box grid and evaluate the integral of Eq. (16) in  $\mathbf{G}$ -space.

### 3.3. Parallelization

Various parallelization strategies for PW-PP calculations have been described in the literature. A strategy that ensures excellent scalability in terms of both computer time and memory consists in distributing the PW basis set and the FFT grid points in real and reciprocal space across processors. A crucial issue for the success of this approach is the FFT algorithm, which must be capable of performing three-dimensional FFT on data shared across different processors with good load balancing. The parallelization in the case of ultrasoft PPs is described in detail in Giannozzi *et al.* [12].

## 4. Applications

Presently, systems described by supercells containing up to a few hundreds atom are within the reach of first-principles MD. A large body of techniques developed for classical MD, such as simulated annealing, finite-temperature simulations, free-energy calculations, etc. can be straightforwardly extended to first-principles MD. Typical applications include the study of aperiodic systems: liquids, atomic clusters, large molecules, including biological active sites; complex solid-state systems: defects in solids, defect diffusion, surface reconstructions; dynamical processes: chemical reactions, catalysis, and finite-temperature studies. The use of ultrasoft PPs is especially convenient in the simulation of systems containing first-row atoms (C, N, O, F) and transition metal elements, such as, e.g., biological active sites, involving Fe, Mn, Ni as catalytic centers.

A good example of application of first-principles MD is the investigation of a complex organometallic reaction: the migratory insertion of carbon monoxide (CO) into zirconium-carbon bonds anchored to a calix[4]arene moiety, shown in Fig. 1 [13]. The investigated reactivity is representative of the large class of migratory insertions of carbon monoxide and alkyl-isocyanides into metal-alkyl bonds observed for most of the early d-block metals, leading to the formation of a new carbon-carbon bond [14].

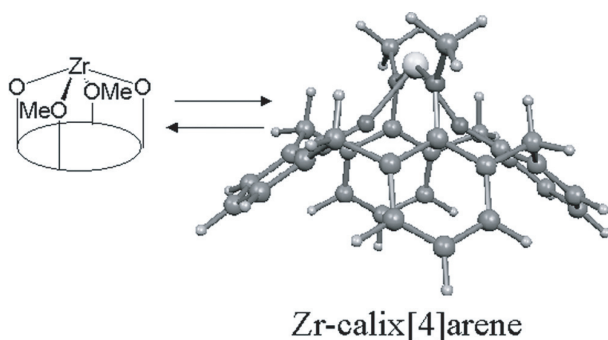


Figure 1. Geometry of calix[4]arene.

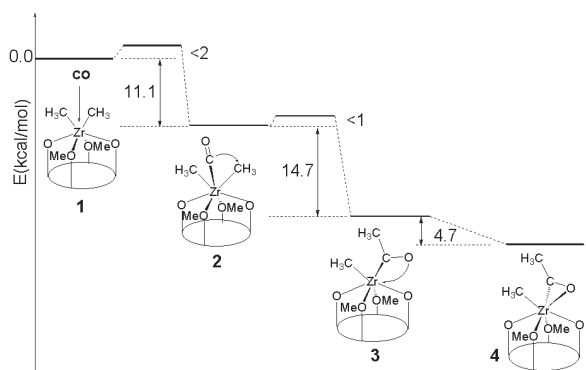


Figure 2. Insertion of CO into the Zr-CH<sub>3</sub> bond of a calix[4]arene.

The CO migratory insertion is supposed to be initialized by the coordination of the nucleophilic CO species to the electron-deficient zirconium centre of [*p*-Bu'<sup>t</sup>calix[4](OMe)<sub>2</sub>(O)<sub>2</sub>-Zr(Me)<sub>2</sub>], **1** in Fig. 2, to form the relatively stable adduct **2**. MD simulations were started by heating up by small steps (via rescaling of atomic velocities) the structure of **2** to a temperature of 300 K. Both electronic and nuclear degrees of freedom were allowed to evolve without any constraint for 2.4 ps.

The migratory CO insertion can be followed by studying the time evolution of the carbon-carbon CH<sub>3</sub>-CO, metal-carbon Zr-CH<sub>3</sub> and metal-oxygen Zr-O distances. Figure 3 clearly shows that the reactive CO migration takes place within ca. 0.4 ps: the fast decrease in the CH<sub>3</sub>-CO distance from ca. 2.7 Å to ca. 1.5 Å corresponds to the formation of the new CH<sub>3</sub>-CO carbon-carbon bond. At the same time the Zr-CH<sub>3</sub> distance follows an almost complementary trajectory with respect to the CH<sub>3</sub>-CO distance and grows from ca. 2.4 up to ca. 3.7 Å, reflecting the methyl detachment from the metal centre upon CO insertion.

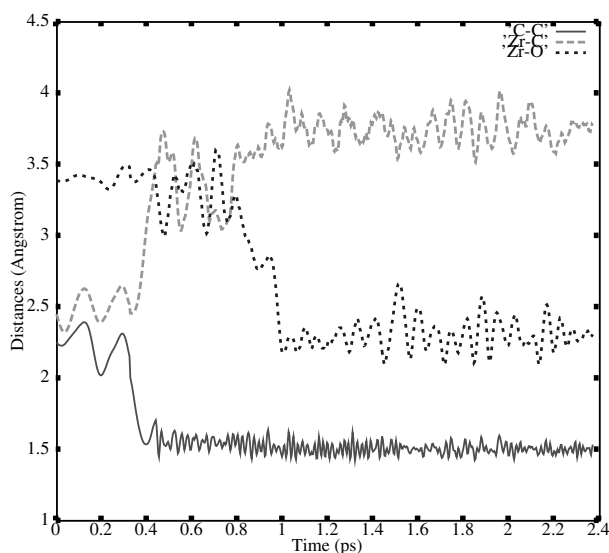


Figure 3. Evolution of carbon–carbon  $\text{CH}_3\text{--CO}$ , metal–carbon  $\text{Zr--CH}_3$  and metal–oxygen  $\text{Zr--O}$  distances during the simulation of CO insertion into calix[4]arene.

The  $\text{Zr--O}$  distance is found to decrease from its initial value of ca.  $3.5 \text{ \AA}$  in **2**, to ca.  $2.2 \text{ \AA}$ , corresponding to the  $\text{Zr--O}$  bond in **4**, within 1.0 ps. The 0.6 ps delay between the formation of the  $\text{CH}_3\text{--CO}$  bond and the formation of the  $\text{Zr--O}$  bond suggests the initial formation of a transient species, **3** in Fig. 2, characterized by an  $\eta^1$ -coordination of the  $\text{OC--CH}_3$  acyl group with a formed  $\text{CH}_3\text{--CO}$  bond and still a long  $\text{Zr--O}$  bond; this  $\eta^1$ -acyl subsequently evolves to the corresponding  $\eta^2$ -bound acyl species. The short time stability of the  $\eta^1$ -acyl isomer (ca. 0.6 ps) suggests a negligible barrier for the conversion of the  $\eta^1$  into the more stable  $\eta^2$ -isomer, as confirmed by static DFT calculations.

## Acknowledgments

Algorithms and codes presented in this work have been originally developed at EPFL Lausanne by Alfredo Pasquarello and Roberto Car, and then at Princeton University by Paolo Giannozzi and Roberto Car. Several people have also contributed or are contributing to the current development and distribution under the GPL License: Kari Laasonen, Andrea Trave, Carlo Cavazzoni, and Nicola Marzari.

## References

- [1] A. Pasquarello, P. Giannozzi, K. Laasonen, A. Trave, N. Marzari, and R. Car, The Car–Parrinello molecular dynamics code described in this paper is freely available in the Quantum-espreso distribution, released under the GNU Public License at <http://www.democritos.it/scientific.php>, 2004.
- [2] D. Vanderbilt, “Soft Self-Consistent Pseudopotentials in a Generalized Eigenvalue Formalism,” *Physical Review B*, 41, 7892, 1990.
- [3] D.R. Hamann, M. Schlüter, and C. Chiang, “Norm-Conserving Pseudopotentials,” *Physical Review Letters*, 43, 1494, 1979.
- [4] K. Laasonen, A. Pasquarello, R. Car, C. Lee, and D. Vanderbilt, “Car–Parrinello Molecular Dynamics with Vanderbilt Ultrasoft Pseudopotentials,” *Physical Review B*, 47, 10142, 1993.
- [5] R. Car and M. Parrinello, “Unified Approach for Molecular Dynamics and Density-Functional Theory,” *Physical Review Letters*, 55, 2471, 1985.
- [6] G. Pastore, E. Smargiassi, and F. Buda, “Theory of Ab Initio Molecular-Dynamics Calculations,” *Physical Review A*, 44, 6334, 1991.
- [7] D. Marx and J. Hutter, “Ab-Initio Molecular Dynamics: Theory and Implementation,” In: *Modern Methods and Algorithms of Quantum Chemistry*, John von Neumann Institute for Computing, FZ Jülich, pp. 301–449, 2000.
- [8] F. Tassone, F. Mauri, and R. Car, “Acceleration Schemes for Ab Initio Molecular-Dynamics Simulations and Electronic-Structure Calculations,” *Physical Review B*, 50, 10561, 1994.
- [9] C. Cavazzoni and G.L. Chiarotti, “A Parallel and Modular Deformable Cell Car–Parrinello Code,” *Computer Physics Communications*, 123, 56, 1999.
- [10] R. Car and M. Parrinello, “The Unified Approach for Molecular Dynamics and Density Functional Theory,” In: A. Polian, P. Loubeyre, and N. Boccara (eds.), *Simple Molecular Systems at Very High Density*, Plenum, New York, p. 455, 1989.
- [11] P. Pulay, “Ab Initio Calculation of Force Constants and Equilibrium Geometries,” *Molecular Physics*, 17, 197, 1969.
- [12] P. Giannozzi, F. De Angelis, and R. Car, “First-Principle Molecular Dynamics with Ultrasoft Pseudopotential: Parallel Implementation and Application to Extended Bio-Inorganic Systems,” *Journal of Chemical Physics*, 120, 5903–5915, 2004.
- [13] S. Fantacci, F. De Angelis, A. Sgamellotti, and N. Re, “Dynamical Density Functional Study of the Multistep CO Insertion into Zirconium–Carbon Bonds Anchored to a Calix[4]arene Moiety,” *Organometallics*, 20, 4031, 2001.
- [14] L.D. Durfee and I.P. Rothwell, “Chemistry of Eta-2-acyl, Eta-2-iminoacyl, and Related Functional Groups,” *Chemical Reviews*, 88, 1059, 1988.